

A Semantic-aware Attention and Visual Shielding Network for Cloth-changing Person Re-identification

Zan Gao, Member, IEEE, Hongwei Wei, Weili Guan, Jie Nie,
Meng Wang, IEEE Fellow, and Shenyong Chen, Senior Member, IEEE, IET Fellow

Abstract - Cloth-changing person reidentification (ReID) is a newly emerging research topic that aims to retrieve pedestrians whose clothes are changed. Since the human appearance with different clothes exhibits large variations, it is very difficult for existing approaches to extract discriminative and robust feature representations. Current works mainly focus on body shape or contour sketches, but the human semantic information and the potential consistency of pedestrian features before and after changing clothes are not fully explored or are ignored. To solve these issues, in this work, a novel semantic-aware attention and visual shielding network for cloth-changing person ReID (abbreviated as SAVS) is proposed where the key idea is to shield clues related to the appearance of clothes and only focus on visual semantic information that is not sensitive to view/posture changes. Specifically, a visual semantic encoder is first employed to locate the human body and clothing regions based on human semantic segmentation information. Then, a human semantic attention module (HSA) is proposed to highlight the human semantic information and reweight the visual feature map. In addition, a visual clothes shielding module (VCS) is also designed to extract a more robust feature representation for the cloth-changing task by covering the clothing regions and focusing the model on the visual semantic information unrelated to the clothes. Most importantly, these two modules are jointly explored in an end-to-end unified framework. Extensive experiments demonstrate that the proposed method can significantly outperform state-of-the-art methods, and more robust features can be extracted for cloth-changing persons. Compared with FSAM (published in CVPR 2021), this method can achieve improvements of 32.7% (16.5%) and 14.9% (-) on the LTCC and PRCC datasets in terms of mAP (rank-1), respectively. When compared with the Swin Transformer, the improvements can reach 28.3% (17.3%), 22.5% (10.0%), 19.5% (10.2%), and 8.6% (10.1%) on the PRCC, LTCC, Celeb, and NKUP datasets in terms of rank-1 (mAP), respectively¹.

Index Terms—Cloth-changing Person Re-identification; Visual Clothes Shielding; Human Semantic Attention; Semantic-aware;

¹Manuscript received April-25th, 2022; This work was supported in part by the National Natural Science Foundation of China (No.61872270, No.62020106004, No.92048301, No.61572357). Young creative team in universities of Shandong Province (No.2020KJN012), Jinan 20 projects in universities (2020GXRC040). New Artificial Intelligence project towards the integration of education and industry in Qilu University of Technology (No.2020KJC-JC01). Shandong project towards the integration of education and industry (No.2022PYI001).

Z. Gao and H.W. Wei (Corresponding author) are with the Shandong Artificial Intelligence Institute, Qilu University of Technology (Shandong Academy of Sciences), Jinan, 250014, P.R China. Z. Gao and S.Y. Chen are also with the Key Laboratory of Computer Vision and System, Ministry of Education, Tianjin University of Technology, Tianjin, 300384, China.

W.L. Guan is with the Faculty of Information Technology, Monash University Clayton Campus, Australia.

J. Nie is with the College of Information Science and Engineering, Ocean University of China, Qingdao 266100, P.R China.

M. Wang is with the school of Computer Science and Information Engineering, Hefei University of Technology, Hefei, 230009, P.R China.



Fig. 1: Examples of cloth-changing person ReID images. The images in each row belong to the same person with different clothes.

I. INTRODUCTION

The person reidentification (ReID) task was first introduced in [1] to explore the usefulness of image retrieval techniques in the public security domain. It is an upstream task of the person detection or person localization tasks, while the ReID task needs to find additional clues about the target person based on the already-acquired perss or video sequences. A typical person ReID system aims to discover matching persons from a gallery library and return the retrieval sequence based on the query probe. Moreover, with the rapid spread of the COVID-19 virus, people often wear face masks in their daily lives, and the face image size in surveillance cameras is often very small; thus, even sophisticated face recognition techniques often fail to recognize the person. To solve this issue, researchers [2], [3], [4], [5], [6], [7], [8], [9], [10], [11], [12], [13], [14], [15], [16] have developed the person ReID technique, which is an important supplement to the face recognition technique, and several person ReID datasets [17], [18], [19] have been released. These approaches are very effective for the person ReID task with short time spans where the human appearance features are fully used for visual matching, but when the surveillance acquisition period becomes longer, the complexity of clothing changes subsequently increases.

Fig. 1 shows some examples of cloth-changing person ReID images, where each row displays the images of the same person wearing different clothes. From them, we can observe that the differences in the visual appearances of the same person with different clothes are very large, and it is also very difficult for humans to identify them. In other words, when data from different cameras are collected for a long time, the appearance of the person’s clothing cannot be used as the feature representation. If the existing person ReID approaches are directly applied in this case, their performance deteriorates dramatically, and they often fail. The reason for this is that the above approaches mainly rely on visual clothing appearance, and they cannot provide a robust feature representation for each identity with different clothes; thus, discriminative and robust feature extraction is an urgent issue for the cloth-changing person ReID task.

To date, a few researchers [20], [21], [22], [23], [24] have made useful attempts for the cloth-changing person ReID task. For example, Huang et al. [20] proposed an augmented representation with vector neurons for cloth-changing. Yang et al. [21] proposed human contour information and polar coordinate transformation to obtain the results of pedestrian matching. Qian et al. [22] proposed a shape embedding module and a clothing-eliminating shape-distillation module. To enrich clothing styles, Zheng et al. [23] proposed a generative adversarial model (GAN) module to expand the training data. Yu et al. [24] proposed a new solution by involving rich clothing templates in training, and in the retrieval, different clothing templates are added into the query in sequence. These approaches are very good for trying to solve the cloth-changing person ReID problem, but since the human appearance exhibits large variations with different clothes, it is very difficult for existing approaches to extract discriminative and robust feature representations. Moreover, current works mainly focus on body shape or contour sketches, but the human semantic information and the potential consistency of pedestrian features before and after changing clothes are not fully explored or are ignored.

To solve these issues, in this work, we propose a novel end-to-end SAVS algorithm for the cloth-changing person ReID task to obtain more discriminative and robust features that are irrelevant to clothes. Extensive experimental results on four cloth-changing person ReID datasets demonstrate that SAVS can outperform state-of-the-art person ReID approaches, and more discriminative and robust features can be obtained that can effectively solve the cloth-changing issue. The main contributions of this paper are summarized as follows.

- We develop a novel end-to-end SAVS network for cloth-changing person ReID that consists of visual semantic encoding and visual semantic decoding. The key idea is to shield clues related to the appearance of clothes and only focus on visual semantic information that is not sensitive to view/posture changes. In this way, the negative effect of the clothing information can be reduced as much as possible.
- We design an HSA module to highlight the human information and reweight the visual feature map that is very helpful for obtaining more discriminative features, and then we develop a VCS module to extract a more robust feature

representation by focusing the model on the visual semantic information unrelated to the clothes. Most importantly, these two modules are jointly explored in an end-to-end unified framework. In this way, more discriminative and robust features can be extracted that are irrelevant to the cloth-changing or pose variants.

- We systematically and comprehensively evaluate the SAVS algorithm on four public cloth-changing person ReID datasets, and the experimental results demonstrate that the SAVS approach can obtain more discriminative and robust features that are irrelevant to clothes; moreover, it can significantly outperform state-of-the-art cloth-changing person ReID methods in terms of the mAP and rank-1.

The remainder of the paper is organized as follows. Section II introduces the related work, and Section III describes the proposed SAVS method. Section IV describes the experimental settings and the analysis of the results. Section V presents the details of the ablation study, and concluding remarks are presented in Section VI.

II. RELATED WORK

To date, many person ReID approaches have been proposed. According to the person’s visual appearance, these methods can be roughly divided into clothing-consistent person ReID and cloth-changing person ReID. In the following, we will separately introduce them.

A. Clothing-Consistent Person ReID

In earlier times, people [25], [23], [26], [27] made efforts to develop related methods for clothing-consistent person ReID where the visual appearance of the clothes was consistent for the same person. For example, Sun et al. [9] proposed a part-based convolutional baseline (PCB) module where a base feature map was first obtained and then equally divided into six feature blocks in the horizontal direction. This method is simple but very effective and has become an important benchmark in the field of person ReID. Wang et al. [13] proposed a multibranch deep network structure (MGN) where one branch is built for the global feature representation and two branches are built for the local feature representation to capture the preference information of the pedestrian identity categories from the whole image. In this way, discriminative information with various granularities can be obtained via an end-to-end feature learning strategy. Gao et al. [15] proposed a deep spatial pyramid-based collaborative feature reconstruction model (DCR) where all blocks of the person were jointly reconstructed; in this way, the issues of occlusion, pose changes, and observation perspective changes can be solved. In addition, some methods employ human skeleton points or human surface texture as a priori knowledge to guide pedestrian reidentification. Song et al. [28] proposed a mask-guided contrastive attention model (MGCAM) to learn features separately from the body and background regions; moreover, a novel region-level triplet loss was designed to restrain the features learned from different regions. Miao et al. [29] proposed a novel pose-guided feature alignment (PGFA) method where a pose estimator was utilized to detect key

points of the human body in pedestrian images, and then these keypoints were used to decide whether a specific body part was occluded. Gao et al. [4] proposed a novel texture semantic alignment (TSA) approach with visibility awareness for the partial person ReID task, where the occlusion issue and changes in poses were simultaneously explored in an end-to-end unified framework. Although these models are robust to changes caused by poses, lighting, and viewing angles, they are vulnerable to clothing changes, as the models heavily rely on the consistency of the appearance of clothes.

B. Cloth-Changing Person ReID

Since the visual appearance of the pedestrians in the cloth-changing person ReID task changes dramatically after a long period, it is very difficult to extract more discriminative and robust feature representations. If the existing clothing-consistent person ReID methods are directly applied to this task, their performance is unsatisfactory. Therefore, to accelerate the development of cloth-changing person ReID techniques, some cloth-changing person ReID datasets have been built and released, such as LTCC [22], PRCC [21], Celeb-reID [20], and NKUP [30]. Moreover, several researchers [20], [21], [22], [31], [32], [33] have made some attempts to address this problem and then assessed their performance on a certain dataset. For example, Yang et al. [21] proposed a SPT+ASE module, where human contour sketching information was used to substitute for human color information. Moreover, a spatial polar transformation (SPT) layer was designed to transform the contour sketch image, and then a multistream network was used to aggregate multiple granular features to better discriminate people by changing the sampling range of the SPT layer. In this way, the changes in visual appearance caused by clothing changes could be reduced. Qian et al. [22] proposed a shape embedding module and a clothing-eliminating shape-distillation module (SE+CESD), where the main idea was to completely delete information related to the appearance of clothes and only focus on body shape information that is not sensitive to changes in perspective and posture. The former was used to encode shape information from human body keypoints, and the latter was utilized to adaptively distill the identity-relevant shape features. Huang et al. [20] designed a ReIDCaps module where a vector neuron concept was proposed. For each vector neuron, its direction was used to represent the changes in clothing information, and its length was utilized to identify the people. In this way, the clothing changes of a specific person can be perceived, and the auxiliary modules can be used to enhance the robustness of the module. Zheng et al. [23] proposed a DG-Net module where a generative model was utilized to automatically generate persons with different appearances regarding clothing. Yu et al. [24] proposed a new solution for changing clothes called COCAS, where rich clothing templates were supplied; thus, in the query, both the clothing template image and an image of the target person wearing other clothes were fed into the module to find the target image. Gao et al. [32] proposed a novel multigranular visual-semantic embedding algorithm (MVSE) for cloth-changing person ReID, where visual semantic information and human attributes are embedded into

the network. Hong et al. [31] proposed a fine-grained shape-appearance mutual learning framework that can learn fine-grained discriminative body shape knowledge in a shaped stream and transfer it to an appearance stream to complement the clothing-unrelated knowledge in the appearance features. Shu et al. [33] proposed a semantic-guided pixel sampling approach for the cloth-changing person re-ID task which forces the model to automatically learn clothing-irrelevant cues that are irrelevant to upper clothes and pants. Gu et al. [41] proposed a Clothes-based Adversarial Loss (CAL) to mine clothes irrelevant features from the original RGB images by penalizing the predictive power of the ReID model. Since the human appearance with different clothes exhibits large variations, it is very difficult for existing approaches to extract discriminative and robust feature representations, and their performances need to be further improved. Moreover, the human semantic information and the potential consistency of pedestrian features before and after changing clothes are not fully explored or are ignored. Thus, in this work, we fully explore the available visual semantic information and the potential consistency of features and then extract a generalized and robust feature to represent a person wearing different clothes.

III. THE PROPOSED APPROACH

As shown in Fig. 2, our proposed SAVS method consists of two stages: a visual semantic encoder and a visual semantic decoder. Moreover, the visual semantic decoder mainly consists of the backbone, the HSA module, and the VCS module, where these three modules are jointly explored in an end-to-end unified framework. In addition, the loss function is used to guide the network optimization. Specifically, an RGB image is first fed into the SCHP [34] module to obtain the human semantic information, the foreground image, and the shielding image, and then the original image, the foreground image, and the shielding image are further fed into the modules of the visual semantic decoder. Note that the enhanced feature, the original feature, and the shielding feature can be obtained in the SAVS, but only the enhanced feature is used in the query. Moreover, the module is focused on human semantic information and visual clothing shielding information; thus, the enhanced feature is more discriminative and robust. In the following, we will introduce the visual semantic encoder, the visual semantic decoder, and the loss function.

A. Visual Semantic Encoder

With the development of deep learning techniques [35], [36], researchers have designed different convolutional neural networks (CNNs) for the person ReID task, but since visual appearances are very different in the cloth-changing person ReID task, it is very difficult for an individual feature to extract a generalized and robust feature to represent a person with different clothes. To accommodate clothing variations within the limited data, enriched feature representations for each identity are needed. Thus, in the visual semantic encoder, the foreground image and the shielding image are generated with the help of human semantic segmentation maps. Specifically,

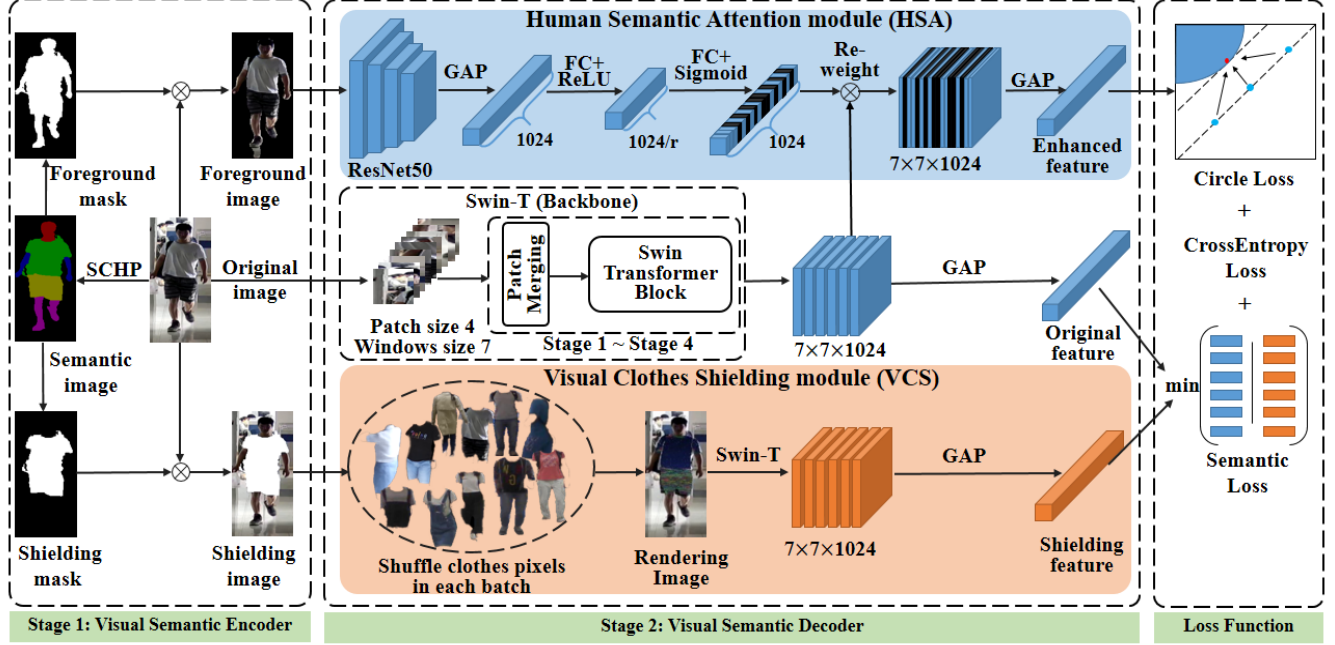


Fig. 2: The pipeline of the SAVS approach is an end-to-end network architecture, and it mainly consists of the visual semantic encoder, the visual semantic decoder, and the loss function. In the visual semantic encoder, the foreground information and visual clothing shielding information are generated for each identity to enrich the image representations. The visual semantic decoder focuses the module on human semantic information and visual clothing shielding information; thus, a more discriminative and robust feature can be extracted. Note that in the SAVS, Swin-T is used as the backbone. GAP indicates the global average pooling, and FC denotes the fully connected layers.

for the original image, the pretrained human parsing SCHK module [34] is employed to obtain the human semantic segmentation information, where the human body is divided into 18 semantic parts. To make it suitable for the cloth-changing person ReID task, these 18 semantic parts are recombined to obtain seven parts, including background, head, torso, pants, arms, legs, and belongings. Figure 3 shows the results of the human semantic segmentation maps. In the following, we provide detailed information on how the foreground image and the visual shielding image can be obtained.

1) The foreground image. Many previous works focus on obtaining the global or local features for each cloth-changing person, but in this work, we pay more attention to the latent association between the foreground and background information, and the foreground image is considered another image representation of the original image. Thus, the key step is to separate the foreground and background for each original image. Based on the human semantic segmentation maps, we perform a binarization process to distinguish between background and nonbackground. All information other than the background is used as the foreground information, such as the torso and legs. Thus, the foreground mask can be obtained. Finally, we associate each body part with its corresponding mask. These pixels inside the mask boundary or outside the mask boundary are considered the foreground image or the background image, respectively. Figure 3 provides the results of the foreground images.

2) Visual shielding image. In the cloth-changing person ReID scenario, the most common change occurs for the upper

clothes and pants. To obtain a more discriminative feature for cloth-changing tasks, the visual shielding image is obtained as another new image representation of the original image by covering the clothing regions of the upper clothes and pants. Specifically, unlike separating foreground information, at this step, finer-grained segmentation labels are required to accurately find the local locations of the upper clothes and pants based on the aforementioned semantic segmentation information. In this way, the shielding mask can be obtained where the pixel value is set to one if it belongs to the mask, or its value is set to zero. Finally, we further combine the original image and the shielding mask by matrix multiplication; thus, the visual shielding image can be obtained. Figure 3 also displays the results of the visual shielding images.

B. Visual Semantic Decoder

The visual semantic decoder mainly consists of the backbone, the HSA module, and the VCS module, where these three modules are jointly explored in an end-to-end unified framework. In our experiments, the Swin Transformer (Swin-T) [37] is used as the backbone to obtain the original feature map $F_o \in R^{7 \times 7 \times 1,024}$, whose input is the original image, and then global average pooling (GAP) is utilized to obtain the original feature $F'_o \in R^{1,024}$. Note that to accommodate person feature extraction, in Swin-T, we set the patch size to 4 for patch partitioning, and we set the window size to 7 for each patch to compute the self-attention inside each window. We keep the transformer blocks from stage 1 to stage 4 to extract visual features and discard the final classification

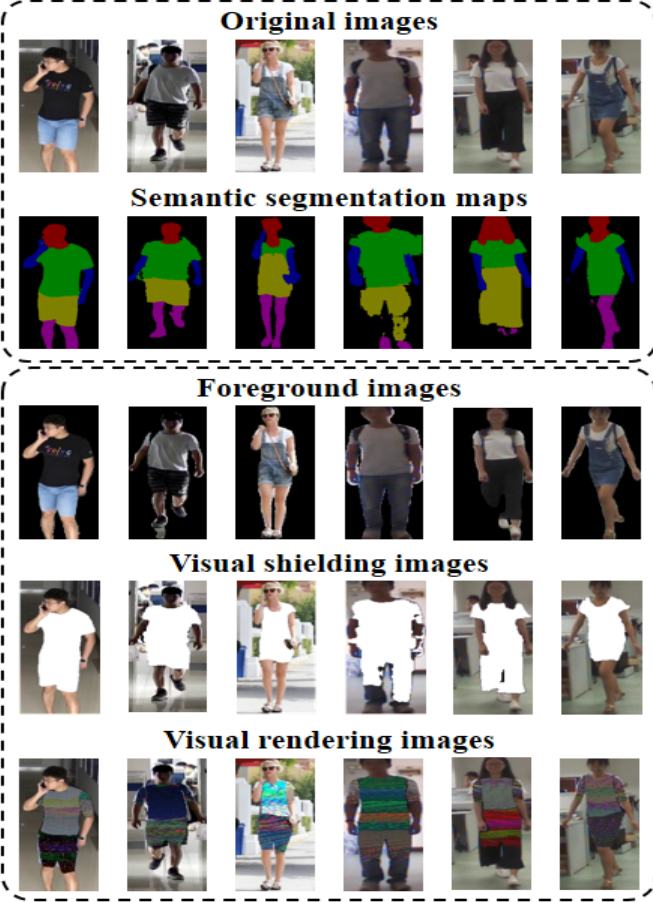


Fig. 3: Results of the visual semantic encoder process. From top to bottom are the original images, the corresponding semantic segmentation maps, the foreground images, the visual shielding images and the visual rendering images.

layer of the network. Moreover, the parameters of the Swin Transformer pre-trained on the ImageNet dataset are further used in the following joint optimization. In the following, we will introduce the HSA and VCS modules separately.

1) Human Semantic Attention Module (HSA). Current works mainly focus on body shape or contour sketches, but human semantic information has not been fully explored. Thus, in this work, an HSA module is designed to highlight the human semantic information and reweight the visual feature map, and the latent correlation between the channels of the convolved features is mined. In this way, the negative effect of the background information can be reduced as much as possible, and more discriminative features can be obtained. The structure of the HSA module is shown in Figure 2. In this module, ResNet50 is used as the basic network architecture, and it is first pretrained on the ImageNet dataset. Then, the parameters of ResNet50 are further jointly optimized with other networks. Specifically, in the HSA module, the feature map $F_A \in R^{7 \times 7 \times 1,024}$ is first obtained by ResNet50, and then it can be further fed into the global average pooling to obtain the feature vector $F'_A \in R^{1024}$. Moreover, the feature vector F'_A is subsequently passed through two fully connected layers, where the first layer is used to obtain a feature representation

with reduced dimensionality ($1,024/r$) (in our experiment, r is set to 16), and the second layer is used to increase the feature dimensionality (1,024). This can be defined as

$$F_w = \sigma\{W_2 \cdot \delta\{W_1 \cdot f_g(F_A)\}\}, \quad (1)$$

$F_w \in R^{1024}$ denotes the weighted feature vector with human semantic information whose input image is the foreground image. f_g indicates the operation of global average pooling. W_1 and W_2 represent the parameters of two fully connected layers. σ and δ indicate the sigmoid activation and the ReLU function, respectively. To make the original feature highlight the human semantic information, the reweight operation is further used for the original feature map $F_o \in R^{7 \times 7 \times 1,024}$ obtained from the original image and the backbone (Swin-T) by the weighted feature vector F_w , and it can be obtained by

$$F'_{e'} = f_g\{F_w \otimes F_o\}, \quad (2)$$

where \otimes denotes the channelwise multiplication between the weight vector F_w and the original feature map F_o . Moreover, the global average pooling operation is used to obtain the feature vector that can describe the persons for subsequent classification training. $F'_{e'} \in R^{1,024}$ indicates the enhanced feature, which is the output of the reweight operation and global average pooling. Since F_w is obtained from the foreground image that can selectively emphasize the human feature channels, $F'_{e'}$ can pay more attention to the human semantic information, and the negative effect of the background information can be reduced as much as possible. Therefore, the extracted feature is more discriminative and robust.

2) Visual Clothes Shielding Module (VCS). In the cloth-changing person ReID scenario, the clothes of the person often change; thus, it will be very difficult to obtain more discriminative features for cloth-changing tasks. We hope that we can extract clothing-irrelevant features where more attention is given to human semantic information; thus, the VCS module is designed, which focuses the model on visual semantic information unrelated to clothes. Specifically, suppose that there are b original images and b corresponding segmentation maps in each batch of the training stage, which can be denoted as $I = [I_1, I_2, \dots, I_i, \dots, I_b]$ and $M = [M_1, M_2, \dots, M_i, \dots, M_b]$, respectively. $I_i \in R^{3 \times H \times W}$ and $M_i \in R^{1 \times H \times W}$ are the original image and the corresponding semantic segmentation map, respectively, and H and W separately denote the height and width. According to these segmentation maps, we can obtain the corresponding clothing regions from the original image; moreover, all pixel values of these clothing regions can also be obtained. To confuse these clothes, we build a shielding pixel pool for each batch where all pixels of these clothing regions are shuffled (the ellipse of Figure 2 shows the pixel pool). Note that in our VCS, we do not care about the pedestrian's upper clothes and pants, and all pixels are equally treated. To reduce the negative effect of the clothes, we specifically transform each pixel of the clothing regions in the original image, and its value is replaced by another value randomly obtained from the shielding pixel pool, but the values of other pixels from nonclothing areas are kept the same as the original image. Finally, the visual rendering image

can be obtained, and its results can be observed in the last row of Figure 3. Then, the visual rendering image is further fed into the Swin Transformer and global average pooling (GAP) to obtain the visual shielding feature $F'_s \in R^{1,024}$, where the network architecture is the same as the backbone of the SAVS, and the shared network parameters with the backbone are employed. Moreover, to make the module focus on the human nonclothing regions, such as the head, face, legs, and feet, we also seek to ensure that the difference between the visual shielding feature and the original feature is as small as possible. In this way, it is difficult for the learning module to differentiate the clothing regions and nonclothing areas, and the clothing-irrelevant features can be extracted, where more attention is devoted to the human semantic information.

C. Loss Function

The person ReID task is often regarded as a person classification problem; thus, the classification loss is often calculated. To further improve the feature discrimination ability of the proposed method, a metric learning loss is added, and it is used to narrow the intraclass distance and increase the interclass loss. Finally, in the HSA module, the human semantic alignment loss is also utilized. Thus, in total, the loss function of the SAVS can be defined as follows:

$$\mathcal{L} = \lambda_1 \mathcal{L}_{id} + \lambda_2 \mathcal{L}_{cir} + \lambda_3 \mathcal{L}_{sem}, \quad (3)$$

where \mathcal{L} is the total loss function of the SAVS, \mathcal{L}_{id} denotes the classification loss, \mathcal{L}_{cir} represents the metric learning loss, and \mathcal{L}_{sem} is the human semantic alignment loss. λ_1 , λ_2 , and λ_3 are the trade-off parameters for balancing the contributions of each term. In our experiments, each term is equally treated; thus, all λ_1 , λ_2 , and λ_3 values are set to 1. Specifically, for the classification loss, the public cross-entropy loss is used as the identity loss to learn discriminative features. To make the feature more discriminative, the circle loss [38] in metric learning is employed to measure the distance between sample pairs. Given a single sample I_e in the feature space, let us assume that there are K intraclass similarity scores and L interclass similarity scores associated with I_e . Moreover, these intraclass similarity scores and interclass similarity scores are denoted as $s_p^i (i = 1, 2, \dots, K)$ and $s_n^j (j = 1, 2, \dots, L)$, respectively. To maximize the intraclass similarity s_p and minimize the interclass similarity, the metric learning loss can be calculated by

$$\begin{aligned} \mathcal{L}_{cir} &= \log[1 + \sum_{i=1}^K \sum_{j=1}^L \exp(\gamma(\alpha_n^j s_n^j - \alpha_p^i s_p^i))], \\ &\quad \begin{cases} \alpha_p^i = [O_p - s_p^i]_+, \\ \alpha_n^j = [s_n^j - O_n]_+, \end{cases} \end{aligned} \quad (4)$$

where α_n^j and α_p^i are nonnegative weighting factors for intraclass similarity scores and interclass similarity scores, respectively. O_p and O_n indicate the optimization score values for s_p^i and s_n^j , respectively. $[*]_+$ indicates the optimization process. γ is the scale factor where the γ values are set to 32 for all similarity scores in our experiments. When a similarity score deviates far from its optimum (i.e., O_n for s_n^j and O_p

for s_p^i), it should obtain a large weighting factor to obtain an effective update with the large gradient. In this way, it can make the learned feature more discriminative.

The clothing regions in the visual rendering image are shielded, whose pixels are replaced by the shielding pixel pool and are very different from those of the original image, but the identity information is retained. Thus, to make the module focus on the human nonclothing regions, such as the head, face, legs, and feet, we also seek to ensure that the difference between the visual shielding feature and the original feature is as small as possible. In this way, the clothing-irrelevant features can be extracted, where more attention is given to the human semantic information. Therefore, the mean square error between the visual shielding feature and the original feature is utilized as the human semantic alignment loss, which can be calculated by

$$\mathcal{L}_{sem} = \frac{1}{b} \sum_{i=1}^b (\|F'_o - F'_s\|_2), \quad (5)$$

where b is the batch size and $\| * \|_2$ indicates the L_2 normalization. $F'_o \in R^{1,024}$ and $F'_s \in R^{1,024}$ denote the original feature and the visual shielding feature, respectively. After optimization, the difference between F'_o and F'_s is very small, and these features focus on the clothing-irrelevant regions of the human. In this way, feature discrimination and generalization can be further improved, and these features can effectively represent people with different clothes.

IV. EXPERIMENTS AND DISCUSSION

To evaluate the performance of our proposed SAVS framework, we perform experiments on four public cloth-changing person ReID datasets: LTCC [22], PRCC [21], Celeb-reID [20], and NKUP [30]. Since the cloth-changing person ReID task is a new and challenging research topic, to the best of our knowledge, at present, there are no comprehensive experiments with any cloth-changing ReID algorithms on all four cloth-changing person ReID datasets, and this is the first work that systematically and comprehensively assesses algorithm performance in the context of these four cloth-changing person ReID datasets. The remainder of this section is organized as follows: 1) the competitors in our experiments are listed, 2) the implementation details are described, and 3) the performance evaluations and comparisons based on these four public datasets are described.

A. Competitors

Since the cloth-changing person ReID task is a new and challenging research topic, only a few works have been published, including SPT+ASE (TPAMI2021) [21], SE+CESD (ACCV 2020) [22], ReIDCaps (TCSVT 2020) [20], Pixel Sampling (ISPL 2021) [33], FSAM (CVPR 2021) [31], and CAL [41] (CVPR 2022). Additionally, in the cloth-changing person ReID task, traditional person ReID algorithms are often employed, such as PCB (ECCV 2018) [9], MGN (ACM MM 2018) [13], ResNet50 (CVPR 2016) [39], DenseNet121 (CVPR 2017) [40], and Swin Transformer (ICCV 2021) [37]. Detailed information can be found in the related work.

TABLE I: Performance evaluation and comparison based on four public cloth-changing person ReID datasets, where the bold values indicate the best performance in each column.

Methods	Datasets							
	LTCC		PRCC		Celeb-reID		NKUP	
	mAP	rank-1	mAP	rank-1	mAP	rank-1	mAP	rank-1
ResNet-50 [39]	8.4	20.7	-	19.4	5.8	43.3	4.9	9.6
DenseNet-121 [40]	10.7	27.2	23.1	18.5	2.9	29.4	3.5	6.6
Swin Transformer [37]	15.2	42.6	47.6	46.9	11.1	46.4	8.5	16.7
PCB [9]	8.8	21.9	-	22.9	8.2	37.1	14.1	18.7
MGN [13]	10.1	24.2	-	25.9	10.8	49.0	16.1	20.6
SE+CESD [22]	11.7	25.2	-	-	-	-	-	-
SPT+ASE [21]	-	-	-	34.4	-	-	-	-
ReIDCaps [20]	-	-	-	-	15.8	63.0	-	-
FSAM [31]	16.2	38.5	-	54.5	-	-	-	-
CAL [41]	18.0	40.1	55.8	55.2	-	-	-	-
Pixel Sampling [33]	16.1	42.3	57.0	63.3	10.2	50.1	8.5	13.9
SAVS (ours)	32.5	71.2	57.6	69.4	21.3	65.9	18.6	25.3

B. Implementation Details

Since the backbone of the SAVS approach is the Swin Transformer, it is also used as the baseline in our experiments. Note that the VCS module is only used in the training stage to jointly optimize the network parameters of the backbone, and in the test stage, only the backbone and the HSA module are used to extract the feature representation where the backbone only focuses on the clothing-irrelevant regions of the human. Finally, only the enhanced feature is used to describe each person, where the original feature is used to reweight the enhanced feature. In addition, the default settings and divisions of these datasets [22], [21], [20], [30] are used. In our experiments, the Swin Transformer is first pretrained on the ImageNet dataset, and then the training samples of the LTCC, PRCC, Celeb-reID, and NKUP datasets are separately used to fine-tune the modules, including Swin Transformer and SAVS. In the training procedure, the minibatch size is set to 32, where each identity has 4 images and the input images are resized to 224×224 . In the optimization process, stochastic gradient descent (SGD) is applied with momentum 0.9, and 60 epochs are required. Moreover, the initial learning rate is set as 3.5×10^{-3} . In addition, the learning rate is decreased by a factor of 0.1 after 40 epochs. Finally, the cumulative matching characteristics (CMCs), rank-1, and mean average precision (mAP) are often utilized as the evaluation metrics in person ReID tasks [21], [15], [20], [33]; thus, we also strictly follow these metrics in our experiments.

C. Performance Evaluations and Comparisons

We first assess the performances of the SAVS method when applied to four public cloth-changing person ReID datasets, and then we compare it with the abovementioned competitors. Among these approaches, if their codes could be obtained, ImageNet was first used to pretrain their backbones, and then the training samples of the LTCC, PRCC, Celeb-reID, and NKUP datasets were separately used to fine-tune the

modules. Finally, the test samples of the four cloth-changing person ReID datasets were separately employed to assess their performances. If the codes were not available, the results reported by the corresponding references were used. Moreover, for a fair comparison, if the performance of a model trained by the training samples is lower than that in the corresponding reference, the results reported by the corresponding reference are also used. The results are shown in Table I. From the table, we can obtain the following observations:

1) The SAVS can achieve the best performance regardless of the dataset and approach used, and large improvements in the mAP and rank-1 values are obtained over those of the state-of-the-art algorithms. For example, when the PRCC dataset is used, the mAP and rank-1 of the SAVS approach are 57.6% and 69.4%, respectively, but the corresponding performances of the baseline are 47.6% and 46.9%, and their corresponding improvements can reach 10.0% (mAP) and 22.5% (rank-1). Similarly, the mAP and rank-1 accuracies of the SAVS approach on the LTCC dataset are 32.5% and 71.2%, respectively, but the corresponding mAP and rank-1 of the baseline can reach 15.2% and 42.6%, where the maximum improvements are 17.3% (mAP) and 28.6% (rank-1). Thus, the SAVS can significantly outperform the baseline. The reason for this is that the HSA and VCS modules are embedded into the Swin Transformer to extract the discriminative and robust features, and then the backbone, HSA, and VCS modules are jointly optimized. In this way, the human semantic information is fully used, and the negative effect of clothing changes is reduced as much as possible. In addition, we also observe that among these approaches, SE+CESD, SPT+ASE, ReIDCaps, FSAM, and Pixel Sampling are specially designed for the cloth-changing person ReID task, but their performance is still worse than that of the SAVS. For example, ReIDCaps has obtained good performance (second place) on the Celeb-reID dataset, where the mAP and rank-1 can reach 15.8% and 63%, respectively, but when comparing it with the SAVS, the improvements of the SAVS can achieve 5.5% (mAP)

and 2.9% (rank-1), respectively. Similarly, when the Pixel Sampling method and the LTCC dataset are used, the mAP and rank-1 on the LTCC dataset are 16.1% and 42.3%, and the improvements of the SAVS can attain 16.4% and 28.9%, respectively. The reason for this is that these specially designed methods mainly focus on body shape or contour sketch, and the complex background and human semantic information are not fully explored or are ignored, but in the SAVS, the HSA and VCS modules are designed to extract clothing-irrelevant features: more attention is given to the human semantic information, and the negative influences of the background and the cloth-changing are reduced as much as possible. Thus, the SAVS experimentally exhibits very good generalization ability, and these experimental results prove the effectiveness and robustness of the SAVS approach.

2) When comparing the clothing-consistent person ReID methods with the cloth-changing person ReID methods, the latter often can obtain much better performance than the former. For example, the MGN can obtain the best performance among the PCB and MGN methods no matter which dataset is utilized, and the Pixel Sampling method is the best among all the clothing-consistent person ReID methods. Thus, in the following, we will compare these two best methods on the different datasets. When the LTCC dataset is employed, the improvements of the Pixel Sampling can reach 22.4% (mAP) and 47% (rank-1). Similarly, when the Celeb-reID dataset is utilized, the mAP and rank-1 of the Pixel Sampling method are improved by 10.5% and 16.9%, respectively. We can draw the same conclusions from the other two datasets. The reason is that since the PCB and MGN methods are specifically designed for clothing-consistent person ReID, they often assume that the same person wears the same clothes within a short time interval, and that their visual appearance must be similar. However, when the cloth-changing issue occurs, the person's appearance shows a large variation; thus, the performance declines dramatically. In the cloth-changing person ReID methods, the key idea is to shield clues related to the appearance of clothes and only focus on visual semantic information that is not sensitive to view/posture changes; thus, the clothing-irrelevant features can be extracted, and their performance is much better than the appearance-relevant features extracted by the clothing-consistent person ReID methods.

3) ResNet50, DenseNet121, and Swin Transformer modules are widely used in many machine learning tasks, but they are also often assessed on the cloth-changing person ReID task. Although these modules can achieve good performances in many related tasks, when they are directly applied to the cloth-changing person ReID task, their performances are unsatisfactory and much worse than that of the SAVS. For example, when the PRCC dataset is used, the rank-1 accuracies of ResNet50, DenseNet121, Swin Transformer, and SAVS are 19.4%, 18.5%, 46.9%, and 69.4%, respectively, and the corresponding improvements achieved by the SAVS method are 50.0%, 50.9%, and 22.5%, respectively. Similarly, the mAP accuracies of ResNet50, DenseNet121, Swin Transformer, and SAVS on the Celeb-reID dataset are 5.8%, 2.9%, 11.1%, and 21.3%, respectively, and the corresponding improvements achieved by the SAVS method are 15.5%, 18.4%, and 10.2%,

respectively. The reason for this is that although these modules are widely used in different tasks, no cloth-changing characteristics are employed in these methods, but in the SAVS, the clothing-irrelevant features are extracted, and the negative influence of the cloth-changing is reduced as much as possible. In addition, from these experiments, we can also observe that the Swin Transformer can achieve the best performance among the ResNet50, DenseNet121, and Swin Transformer modules no matter which dataset is used; thus, in our experiments, the Swin Transformer is also used as the backbone of the SAVS.

V. ABLATION STUDY

An ablation study is performed using the SAVS model to analyze the contribution of each component. In this investigation, four aspects are considered: 1) the effectiveness of the HSA module, 2) the advantages of the VCS module, 3) a convergence analysis, and 4) a qualitative visualization. In the following, we discuss these four aspects separately.

A. Effectiveness of the HSA Module

In the few existing cloth-changing person ReID methods, the global or local features are often extracted to represent the cloth-changing person, but in this section, we assess the effectiveness of the HSA module on four public cloth-changing person ReID datasets where the importance of human semantic information is discussed. Since the Swin Transformer is the backbone of the SAVS, in our experiments, it is also used as the baseline, where the Swin Transformer is used to extract features from the original image, and then the Softmax is used as the classification function. To assess the effectiveness of the original image, the foreground image, and the background image, this basic network is also used to extract the feature representations for them, and then these features are employed to find the persons from the gallery dataset. Finally, we name them 'O', 'F', and 'B', respectively. To further evaluate the importance of human semantic information, the human semantic information (the foreground image) is fed into the HSA module, and then its outputs are used to reweight the original feature extracted by the Swin Transformer and the original image (we name it 'O+F'). Similarly, the background image is fed into the HSA module in place of the foreground image, and the reweight operation is also used for the original feature (we call this method 'O+B'). Their results are given in Table II and Figure 4. From them, we can make the following observations.

1) The original image can achieve the best performance when only the baseline is used, and the foreground image and the background image can obtain second and third places, respectively. For example, the mAP and rank-1 accuracies of the original image are 15.2% and 42.6%, respectively, on the LTCC dataset, and the corresponding accuracies of the foreground image are 11.7% and 34.3%, but the corresponding accuracies of the background image are 10.2% and 14.7%, respectively; thus, the performance of the original image can outperform the foreground and background images. Similarly, when the Celeb-reID dataset is used, the rank-1 accuracies of the original, foreground, and background images are 46.4%,

TABLE II: Effectiveness of the HSA module where four public cloth-changing person ReID datasets are employed, and the bold values indicate the best performance in each column. Note that O , F , and B indicate the original image, the foreground image, and the background image, respectively.

Components	Datasets							
	O	F	B	LTCC	PRCC	Celeb-reID	NKUP	
				mAP	rank-1	mAP	rank-1	
✓	15.2	42.6		47.6	46.9	11.1	46.4	
✓		11.7	34.3	40.0	45.2	9.8	40.0	
✓		✓	10.2	14.7	20.8	16.9	1.2	7.4
✓	✓		17.9	44.3	50.7	45.2	9.8	49.7
✓	✓	✓	24.4	56.0	54.0	60.3	15.9	59.1

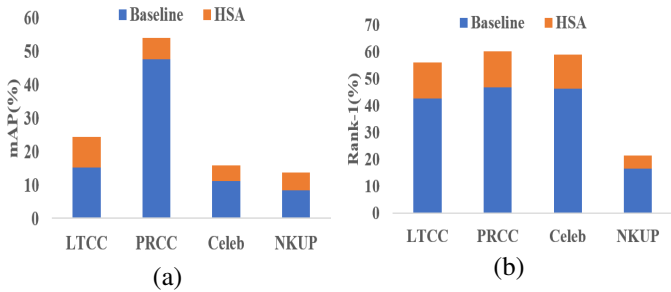


Fig. 4: Advantages of the HSA module, where four public cloth-changing datasets are utilized, and the evaluation metrics of mAP and rank-1 are used in (a) and (b), respectively. Note that the blue bar indicates the results of the baseline, and the yellow bar denotes the improvements over the baseline when the HSA module is further used.

40.0%, and 7.4% and the improvement of ‘ O ’ can reach 6.4% (‘ F ’) and 39% (‘ B ’), respectively. Although person ReID is a cross-scene retrieval task and we usually assume that the background information is useless, the experimental results show that the performance of the foreground image is worse than that of the original image no matter which dataset is used. For example, when the PRCC dataset is used, the mAP accuracies of the former and latter are 47.6% and 40.0%, respectively, whose improvement can reach 7.6%. Thus, these experimental results prove that the foreground image is very useful, but the background information cannot be eliminated in its entirety.

2) The performance of ‘ $O+F$ ’ can obtain a large improvement when compared with ‘ O ’ or ‘ F ’ regardless of the dataset used. For example, on the LTCC dataset, the mAP accuracies of ‘ $O+F$ ’, ‘ O ’, and ‘ F ’ are 24.4%, 15.2%, and 11.7%, respectively, whose improvements can be 9.2% and 12.7%. When the PRCC dataset is used, the rank-1 accuracies of ‘ $O+F$ ’, ‘ O ’, and ‘ F ’ can reach 60.3%, 46.9%, and 45.2%, respectively, and the improvement of ‘ $O+F$ ’ can achieve 13.4% and 15.1%. The reason for this is that in ‘ $O+F$ ’, the HSA module is used to emphasize the importance of the human semantic information and reweight the visual feature map extracted by the original image. In this way, the negative effect of the background information can be reduced as much as possible, and more discriminative features can be obtained. In addition,

TABLE III: Benefits of the VCS, where four public cloth-changing datasets are utilized. Notice that the Swin Transformer is used as the baseline, and our proposed HSA and VCS modules are embedded into the baseline step by step.

Methods	Datasets					
	LTCC		PRCC		Celeb-reID	
	mAP	rank-1	mAP	rank-1	mAP	rank-1
Baseline	15.2	42.6	47.6	46.9	11.1	46.4
+HSA	24.4	56.0	54.0	60.3	15.9	59.1
+HSA+VCS	32.5	71.2	57.6	69.4	21.3	65.9
					18.6	25.3

we also observe that when the background information is fed into the HSA module, the performance of ‘ $O+B$ ’ is not stable on different datasets; for example, when the PRCC and NKUP datasets are used, the rank-1 accuracies of ‘ $O+B$ ’ are worse than those of ‘ O ’, but on other datasets, the rank-1 accuracies of ‘ $O+B$ ’ can obtain little improvement. From Figure 4, we can also obtain the same conclusions. Thus, these experiments demonstrate that the HSA module is very effective for enriching the feature representation, and the human semantic information is very helpful for feature extraction. In addition, the background information is somewhat useful for the feature representation, but emphasizing background information cannot always obtain a performance increase.

B. Advantages of the VCS Module

To validate the advantages of the VCS module, we perform experiments on the four public cloth-changing person ReID datasets, and their results are given in Table III and Figure 5. Note that in Table III, when the original image is fed into the Swin Transformer, the module is considered the baseline. Moreover, when the foreground image (human semantic) is further fed into the HSA module and its results are combined with the backbone, it is called ‘+HSA’. Finally, when the VCS module is further used, the visual clothing shielding image is further embedded into the ‘+HSA’ module; thus, we name it ‘+HSA+VCS’. From them, we can see that

1) When the VCS module is used, the performance of ‘+HSA+VCS’ can be greatly improved over that of the ‘+HSA’ module. For example, when the Celeb-reID dataset is used, the mAP and rank-1 accuracies of ‘+HSA+VCS’ are 21.3% and 65.9%, and the mAP and rank-1 accuracies of ‘+HSA’ are 15.9% and 59.1%, respectively, whose improvements can reach 5.4% (mAP) and 6.8% (rank-1). On the PRCC dataset, the rank-1 accuracies of ‘+HSA+VCS’ and ‘+HSA’ are 60.3% and 69.4%, and the improvement can reach 9.1%. We can draw similar conclusions from the other datasets. In addition, when the CMC curves are used as the metric, we can also observe the same results in Figure 5. The reason why the VCS module can be successful is that visual clothing shielding makes it difficult for appearance features to be learned, and thus, the model loses its reliance on clothing appearance when extracting features. Through the contrastive learning of the original and visual shielding features, the potential consistency can be explored to effectively solve the cloth-changing problem.

2) In the SAVS module, the original image information, visual shielding information, and human semantic information

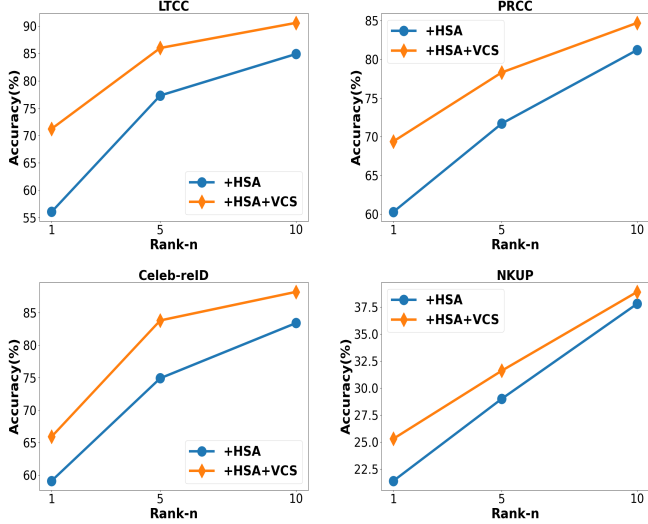


Fig. 5: Advantage analysis of the VCS module by using CMC curves on the LTCC, PRCC, Celeb-reID and NKUP datasets.

are jointly learned in a unified framework. These modules are complementary, and they can promote each other. When the HSA module and the VCS module are embedded into the baseline step by step, their combined performance can yield a stable improvement. For example, when the LTCC dataset is used, the mAP (rank-1) accuracies of the baseline, ‘+HSA’, and ‘+HSA+VCS’ are 15.2% (42.6%), 24.4% (56%), and 32.5% (71.2%), respectively, whose performance can be improved step by step, and the improvement of the ‘+HSA+VCS’ can achieve 17.3% (13.4%, baseline) and 9.2% (28.6%, ‘+HSA’). Similarly, on the PRCC dataset, the corresponding improvements of the ‘+HSA+VCS’ module can reach 6.4% (13.4%, baseline) and 10% (23.5%, ‘+HSA’), respectively.

3) In the SAVS and Pixel Sampling, both focus on the surface features of clothes; thus, we also compare their performance on two widely used public datasets, including LTCC and Celeb-reID. Since ResNet-50 is the backbone of Pixel Sampling, to obtain a fair comparison, ResNet-50 is also used as the backbone in the SAVS, but the human semantic information is ignored, and we call this approach ‘ResNet50+VCS’. Along another line, to assess the advantages of the backbone, the backbone of the SAVS is replaced with the Swin Transformer based on the ‘ResNet50+VCS’, and we name this approach ‘Swin-T+VCS’. Finally, the HSA module is further assessed, and the human semantic information is embedded into ‘Swin-T+VCS’, whose name is ‘Swin-T+VCS+HSA’. Their results are shown in Table IV. From this, we can observe that when the same backbone and training strategy is used in the Pixel Sampling and the ‘ResNet50+VCS’, the performance of the latter is much better than that of the former. For example, the mAP (rank-1) accuracies of the ‘ResNet50+VCS’ and Pixel Sampling on the LTCC dataset are 18.7% (47.7%) and 16.1% (42.3%), respectively, whose improvement can reach 2.6% (5.4%). We can obtain the same results from the Celeb-reID dataset. The reason why the ‘ResNet50+VCS’ is much better than the Pixel

TABLE IV: Advantage of the VCS and backbone on the LTCC and Celeb-reID datasets when compared with the Pixel Sampling method.

Methods	LTCC		Celeb-reID	
	mAP	rank-1	mAP	rank-1
Pixel Sampling [33]	16.1	42.3	10.2	50.1
ResNet50+VCS	18.7	47.7	11.6	52.8
Swin-T+VCS	22.8	54.9	15.2	57.9
Swin-T+VCS+HSA	32.5	71.2	21.3	65.9

Sampling is that the latter only focuses on a single item of clothing, but all clothing regions of the person are fully considered in the former. In this way, the negative effect of cloth-changing can be reduced as much as possible, and a more robust feature representation can be extracted by covering the clothing regions and focusing the model on the visual semantic information unrelated to the clothes. Thus, these experiments can further prove that the VCS module is very effective for solving the cloth-changing issue. In addition, when the Swin Transformer is further used, we can see that the performance can be further improved. For example, on the LTCC dataset, the mAP (rank-1) accuracies of ‘Swin-T+VCS’ and Pixel Sampling are 22.8% (54.9%) and 16.1% (42.3%), respectively, whose improvement can reach 6.7% (12.6%). Thus, it can be proven that the Swin Transformer is also very efficient, and in our following experiments, it is utilized as the backbone of the SAVS. Finally, when the HSA module is further employed, its performance can significantly outperform the baseline, the Pixel Sampling, ‘ResNet50+VCS’, and ‘Swin-T+VCS’ regardless of datasets.

C. Convergence Analysis

In this section, we evaluate the convergence of the proposed SAVS method on four public cloth-changing person ReID datasets, including LTCC, PRCC, Celeb-reID, and NKUP, and their convergence curves are shown in Figure 6. From this figure, we can observe that the convergence speeds of the SAVS method are very fast no matter which dataset is utilized. Moreover, in the optimization process, only 30-40 epochs are required for all datasets, and the convergence curves can be stable regardless of the dataset utilized. Thus, this can further prove the effectiveness of the SAVS method.

D. Qualitative Visualization

To further prove the effectiveness and robustness of the SAVS, in this section, we visualize some results of the proposed SAVS on the different datasets. In this investigation, three aspects are considered: 1) visualization of the attention maps, 2) visualization of the similarity map, and 3) qualitative visualization of the retrieval results. In the following, we discuss these three aspects separately, and their results are given in Figures 7, 8, 9, and 10. From them, we can make the following observations.

1) To further illustrate which part of the focused features are learned with the help of different modules in the SAVS,

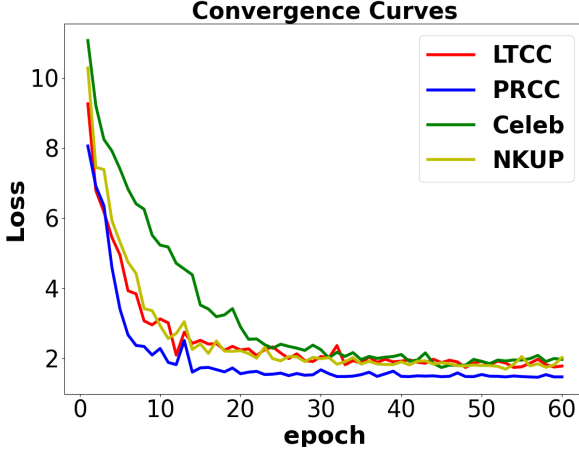


Fig. 6: Convergence curves of the SAVS method for the LTCC, PRCC, Celeb-reID and NKUP datasets.

the attention maps are visualized and displayed in Figure 7. In this figure, the first row indicates the original images from different datasets. The second row ('+HSA') represents which channels on the feature map are activated by the reweighting operation where the Swin Transformer and the HSA module are used. The third row ('+HSA+VCS') denotes which channels between the original features and visual shielding features are more consistently constrained by the semantic alignment loss and the VCS module, where the Swin Transformer, the HSA, and VCS modules are utilized. From them, we can see that in the second row, the human semantic attention module is utilized; thus, only the human semantic channels are activated where the activated regions focus on the human body, but the background information is largely ignored. Thus, these channels (corresponding to features that play a major role in later classification) are enhanced, and more discriminative and robust features can be extracted. From the third row, we can observe that the VCS module focuses on human body nonclothing regions, e.g., head, face, legs, arms, shoes, and belongings, and the human clothing regions are ignored; thus, the extracted features are clothing-irrelevant, which can effectively solve the issue of human cloth-changing, and a more discriminative and robust feature representation can be obtained. Thus, these experiments can further prove the effectiveness and advantages of the HSA and VCS modules.

2) To intuitively illustrate the effectiveness of the HSA and VCS modules from another view, the feature similarities between different images are calculated. Specifically, 14 images of the same person wearing different clothes are first selected, and then the features are extracted for each image by the Swin Transformer (our baseline). Moreover, the cosine similarities between any two images are calculated by the corresponding features. Finally, we repeat the above operation in pairs for all 14 images and visualize their similarities to obtain a 14×14 similarity map. Similarly, we can also extract these image features by Swin Transformer+HSA+VCS (our proposed SAVS module), and then the cosine similarities between them and the similarity map are calculated. The results are given in Figure 8, where the blue and green colors

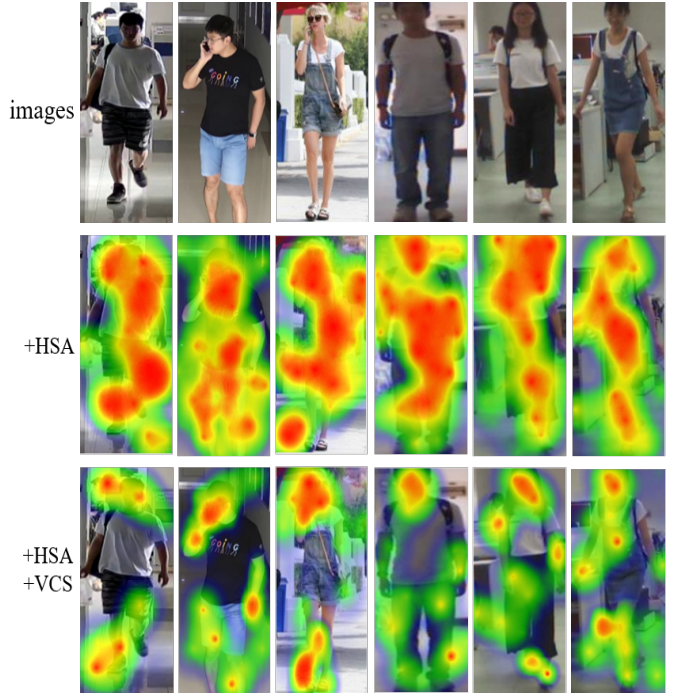


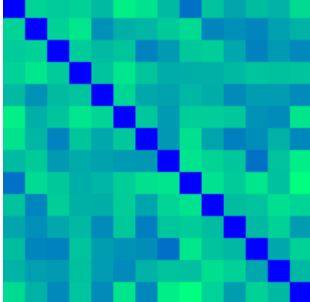
Fig. 7: Visualization of attention maps. The first row, second row, and third row indicate the original images, the results of '+HSA', and the results of '+HSA+VCS', respectively. The '+HSA' focuses on the human body region, and the '+HSA+VCS' focuses on clothing-irrelevant cues, e.g., head, legs, and shoes.

represent the most and the least similar pairs, respectively. From this, we can determine that when only the baseline is utilized, the extracted features are very relative to the clothes, and the features are not discriminative and robust; thus, the similarities between the same person wearing different clothes are very small (the color of most of the squares is green). However, when the HSA and VCS modules are embedded into the baseline, the human semantic information and the clothing-irrelevant clues are fully explored; thus, the extracted features are more discriminative and robust, where similarities between the same person wearing different clothes are added, and the color of most of the squares is blue. Thus, these experiments can further prove that the SAVS is very effective, efficient, and robust.

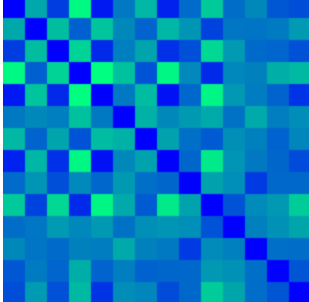
3) To further prove the effectiveness and robustness of the SAVS method, in this section, the retrieval results of the SAVS on the PRCC and NKUP datasets are given in Figures 9 and 10, respectively, where each row is a retrieval example including one query image and the top ten most similar images. We notice that in Figure 9, the effectiveness of different parts of the SAVS, including (a) the baseline, (b) the baseline+HSA, and (c) the baseline+HSA+VCS, is visualized with respect to the PRCC dataset. Figure 9 demonstrates that since the visual appearance of the cloth-changing person drastically changes, the baseline still has difficulty obtaining the correct retrieval results when only the original feature is extracted. When the human semantic information is further combined, the feature discrimination is improved. Although the number of correct retrieval results is increased significantly,



(a) 14 images of the same person wearing different clothes



(b) similarity map without the HSA and VCS modules



(c) similarity map with the HSA and VCS modules

Fig. 8: Similarity maps with or without ‘+HSA+VCS’. The cosine similarity is used to calculate the distance between two images. The color of each square represents the degree of similarity between the two images indicated by the horizontal and vertical coordinates. The blue and green colors represent the most and the least similar pairs, respectively.



Fig. 9: Qualitative visualization of a) baseline, b) baseline+HSA, and c) baseline+HSA+VCS (SAVS) on the PRCC dataset. The top left column is a single query image, and the other columns represent the top ten retrieval results. Note that the red boxes indicate the correct results.

the first correct retrieval result lies in the third position, and the average performance is not unsatisfactory. Finally, when visual shielding information is employed, more correct retrieval results can be returned; moreover, their locations are very close to the front of the images. Thus, these results can further prove that the HSA and VCS modules are very useful for describing cloth-changing persons, and the extracted feature is effective and robust. To further demonstrate the effectiveness of the SAVS modules on difficult samples, we visualize four retrieval results of the SAVS module on the NKUP dataset, where the face information is often covered, and the results are presented in Figure 10. In the two retrieval cases of a) and b), the full-frontal image is given, but in the gallery, the facial information of one person is often obscured in (a), and the person is captured with mainly back profile information in (b). Luckily, in this case, the SAVS can still



Fig. 10: Qualitative visualization of the SAVS on the NKUP dataset. The top left column is a single query image, and the other columns represent the top ten retrieval results. Note that the red boxes indicate the correct results.

retrieve 4-5 correct results effectively, and these results are also at the top of the returned results. In both retrieval cases c) and d), where the provided image is a back image or the face is obscured, the SAVS can still correctly identify persons, but the average result declines dramatically, where only one or two correct results are returned. These experimental results indicate that it is quite challenging to perform cloth-changing person reidentification when the provided image lacks visual semantics to a large extent.

VI. CONCLUSION

This work proposed a novel SAVS algorithm for the cloth-changing person ReID task, where the key idea is to shield clues related to the appearance of clothes and only focus on visual semantic information that is not sensitive to view/posture changes. In the SAVS, an HSA module is designed to highlight human information and reweight the visual feature map, and a VCS module is proposed to extract a more robust feature representation for cloth-changing tasks by covering clothing regions and focusing the model on visual semantic information unrelated to clothes. Most importantly, these two modules are jointly explored in an end-to-end unified framework. The results of extensive experiments conducted on four cloth-changing person ReID datasets demonstrate that the SAVS can significantly outperform state-of-the-art cloth-changing person ReID methods in terms of both mAP and rank-1 accuracy, and more discriminative and robust features can be extracted to represent the cloth-changing persons. An ablation study also proves that human semantic information and visual shielding information are very helpful for solving the cloth-changing person ReID task where clothes-independent features can be obtained. Additionally, different qualitative visualizations can further prove the effectiveness and robustness of the HSA and VCS modules.

In the future, we intend to explore how to shield the effects of clothing changes and design approaches based on novel

dynamic features such as gait that can also describe static persons.

REFERENCES

- [1] L. Zheng, Y. Yang, and A. G. Hauptmann, "Person re-identification: Past, present and future," *CoRR*, vol. abs/1610.02984, 2016. I
- [2] C. Zhao, X. Lv, S. Dou, S. Zhang, J. Wu, and L. Wang, "Incremental generative occlusion adversarial suppression network for person reid," *IEEE Trans. Image Process.*, vol. 30, pp. 4212–4224, 2021. I
- [3] Z. Zheng, L. Zheng, and Y. Yang, "Pedestrian alignment network for large-scale person re-identification," *IEEE Transactions on Circuits and Systems for Video Technology*, vol. 29, no. 10, pp. 3037–3045, 2019. I
- [4] L. Gao, H. Zhang, Z. Gao, W. Guan, Z. Cheng, and M. Wang, "Texture semantically aligned with visibility-aware for partial person re-identification," in *MM '20: The 28th ACM International Conference on Multimedia, Virtual Event / Seattle, WA, USA, October 12–16, 2020*, pp. 3771–3779. I, II-A
- [5] R. R. Varior, G. Wang, J. Lu, and T. Liu, "Learning invariant color features for person reidentification," *IEEE Trans. Image Process.*, vol. 25, no. 7, pp. 3395–3410, 2016. I
- [6] Y. Lin, L. Zheng, Z. Zheng, Y. Wu, Z. Hu, C. Yan, and Y. Yang, "Improving person re-identification by attribute and identity learning," *Pattern Recognit.*, vol. 95, pp. 151–161, 2019. I
- [7] J. Yang, W. Zheng, Q. Yang, Y. Chen, and Q. Tian, "Spatial-temporal graph convolutional network for video-based person re-identification," in *IEEE Conference on Computer Vision and Pattern Recognition, Seattle, WA, USA, June 13–19, 2020*, pp. 3286–3296. I
- [8] L. Wei, S. Zhang, H. Yao, W. Gao, and Q. Tian, "GLAD: global-local-alignment descriptor for scalable person re-identification," *IEEE Transaction on Multimedia*, vol. 21, no. 4, pp. 986–999, 2019. I
- [9] Y. Sun, L. Zheng, Y. Yang, Q. Tian, and S. Wang, "Beyond part models: Person retrieval with refined part pooling (and a strong convolutional baseline)," in *Proceedings of the European conference on computer vision (ECCV)*, 2018, pp. 480–496. I, II-A, IV-A, I
- [10] B. Sun, Y. Ren, and X. Lu, "Semisupervised consistent projection metric learning for person reidentification," *IEEE Trans. Cybern.*, vol. 52, no. 2, pp. 738–747, 2022. I
- [11] Y. Sun, L. Zheng, Y. Li, Y. Yang, Q. Tian, and S. Wang, "Learning part-based convolutional features for person re-identification," *IEEE Trans. Pattern Anal. Mach. Intell.*, vol. 43, no. 3, pp. 902–917, 2021. I
- [12] A. J. Ma, J. Li, P. C. Yuen, and P. Li, "Cross-domain person reidentification using domain adaptation ranking svms," *IEEE Trans. Image Process.*, vol. 24, no. 5, pp. 1599–1613, 2015. I
- [13] G. Wang, Y. Yuan, X. Chen, J. Li, and X. Zhou, "Learning discriminative features with multiple granularities for person re-identification," in *Proceedings of the 26th ACM international conference on Multimedia*, 2018, pp. 274–282. I, II-A, IV-A, I
- [14] H. Wang, L. Jiao, S. Yang, L. Li, and Z. Wang, "Simple and effective: Spatial rescaling for person reidentification," *IEEE Trans. Neural Networks Learn. Syst.*, vol. 33, no. 1, pp. 145–156, 2022. I
- [15] Z. Gao, H. Zhang, L. Gao, Z. Cheng, and S. Chen, "Dcr: A unified framework for holistic/partial person reid," *IEEE Transactions on Multimedia*, vol. 23, pp. 3323–3345, 2021. I, II-A, IV-B
- [16] M. Ye, J. Shen, G. Lin, T. Xiang, L. Shao, and S. C. Hoi, "Deep learning for person re-identification: A survey and outlook," *IEEE Transactions on Pattern Analysis and Machine Intelligence*, pp. 1–1, 2021. I
- [17] L. Zheng, L. Shen, L. Tian, S. Wang, J. Wang, and Q. Tian, "Scalable person re-identification: A benchmark," in *IEEE International Conference on Computer Vision*, 2015, pp. 1116–1124. I
- [18] Z. Zheng, L. Zheng, and Y. Yang, "Unlabeled samples generated by gan improve the person re-identification baseline in vitro," in *Proceedings of the IEEE International Conference on Computer Vision*, 2017, pp. 3754–3762. I
- [19] W. Li, R. Zhao, T. Xiao, and X. Wang, "Deepreid: Deep filter pairing neural network for person re-identification," in *Proceedings of the IEEE conference on computer vision and pattern recognition*, 2014, pp. 152–159. I
- [20] Y. Huang, J. Xu, Q. Wu, Y. Zhong, P. Zhang, and Z. Zhang, "Beyond scalar neuron: Adopting vector-neuron capsules for long-term person re-identification," *IEEE Trans. Circuits Syst. Video Technol.*, vol. 30, no. 10, pp. 3459–3471, 2020. I, II-B, II-B, II-B, IV, IV-A, I, IV-B, IV-B
- [21] Q. Yang, A. Wu, and W.-S. Zheng, "Person re-identification by contour sketch under moderate clothing change," *IEEE Transactions on Pattern Analysis and Machine Intelligence*, vol. 43, no. 6, pp. 2029–2046, 2021. I, II-B, II-B, II-B, IV, IV-A, I, IV-B, IV-B
- [22] X. Qian, W. Wang, L. Zhang, F. Zhu, Y. Fu, T. Xiang, Y.-G. Jiang, and X. Xue, "Long-term cloth-changing person re-identification," in *Proceedings of the Asian Conference on Computer Vision*, 2020. I, II-B, II-B, II-B, IV, IV-A, I, IV-B
- [23] Z. Zheng, X. Yang, Z. Yu, L. Zheng, Y. Yang, and J. Kautz, "Joint discriminative and generative learning for person re-identification," in *Proceedings of the IEEE Conference on Computer Vision and Pattern Recognition*, 2019, pp. 2138–2147. I, II-A, II-B
- [24] S. Yu, S. Li, D. Chen, R. Zhao, J. Yan, and Y. Qiao, "Cocas: A large-scale clothes changing person dataset for re-identification," in *Proceedings of the IEEE Conference on Computer Vision and Pattern Recognition*, 2020, pp. 3400–3409. I, II-B
- [25] H. Yao, S. Zhang, R. Hong, Y. Zhang, C. Xu, and Q. Tian, "Deep representation learning with part loss for person re-identification," *IEEE Transactions on Image Processing*, vol. 28, no. 6, pp. 2860–2871, 2019. II-A
- [26] S. Paisitkriangkrai, C. Shen, and A. Van Den Hengel, "Learning to rank in person re-identification with metric ensembles," in *Proceedings of the IEEE Conference on Computer Vision and Pattern Recognition*, 2015, pp. 1846–1855. II-A
- [27] Y. Shen, T. Xiao, H. Li, S. Yi, and X. Wang, "End-to-end deep kronecker-product matching for person re-identification," in *Proceedings of the IEEE conference on computer vision and pattern recognition*, 2018, pp. 6886–6895. II-A
- [28] C. Song, Y. Huang, W. Ouyang, and L. Wang, "Mask-guided contrastive attention model for person re-identification," in *Proceedings of the IEEE Conference on Computer Vision and Pattern Recognition*, 2018, pp. 1179–1188. II-A
- [29] J. Miao, Y. Wu, P. Liu, Y. Ding, and Y. Yang, "Pose-guided feature alignment for occluded person re-identification," in *Proceedings of the IEEE International Conference on Computer Vision*, 2019, pp. 542–551. II-A
- [30] K. Wang, Z. Ma, S. Chen, J. Yang, K. Zhou, and T. Li, "A benchmark for clothes variation in person re-identification," *International Journal of Intelligent Systems*, vol. 35, no. 12, pp. 1881–1898, 2020. II-B, IV, IV-B
- [31] P. Hong, T. Wu, A. Wu, X. Han, and W. Zheng, "Fine-grained shape-appearance mutual learning for cloth-changing person re-identification," in *IEEE Conference on Computer Vision and Pattern Recognition, CVPR, virtual, June 19–25, 2021*, pp. 10 513–10 522. II-B, II-B, IV-A, I
- [32] Z. Gao, H. Wei, W. Guan, W. Nie, M. Liu, and M. Wang, "Multigranular visual-semantic embedding for cloth-changing person re-identification," *CoRR*, vol. abs/2108.04527, 2021. II-B, II-B
- [33] X. Shu, G. Li, X. Wang, W. Ruan, and Q. Tian, "Semantic-guided pixel sampling for cloth-changing person re-identification," *IEEE Signal Process. Lett.*, vol. 28, pp. 1365–1369, 2021. II-B, II-B, IV-A, I, IV-B, IV
- [34] P. Li, Y. Xu, Y. Wei, and Y. Yang, "Self-correction for human parsing," *CoRR*, vol. abs/1910.09777, 2019. III, III-A
- [35] Z. Liu, S. Wu, S. Jin, Q. Liu, S. Lu, R. Zimmermann, and L. Cheng, "Towards natural and accurate future motion prediction of humans and animals," in *IEEE Conference on Computer Vision and Pattern Recognition*, 2019, pp. 10 004–10 012. III-A
- [36] Z. Gao, L. Guo, W. Guan, A. Liu, T. Ren, and S. Chen, "A pairwise attentive adversarial spatiotemporal network for cross-domain few-shot action recognition," *IEEE Transactions on Image Processing*, vol. 30, pp. 767–782, 2021. III-A
- [37] Z. Liu, Y. Lin, Y. Cao, H. Hu, Y. Wei, Z. Zhang, S. Lin, and B. Guo, "Swin transformer: Hierarchical vision transformer using shifted windows," in *IEEE/CVF International Conference on Computer Vision, ICCV, Montreal, QC, Canada, October 10–17, 2021*, pp. 9992–10 002. III-B, IV-A, I
- [38] Y. Sun, C. Cheng, Y. Zhang, C. Zhang, L. Zheng, Z. Wang, and Y. Wei, "Circle loss: A unified perspective of pair similarity optimization," in *IEEE/CVF Conference on Computer Vision and Pattern Recognition, CVPR, Seattle, WA, USA, June 13–19, 2020*, pp. 6397–6406. III-C
- [39] K. He, X. Zhang, S. Ren, and J. Sun, "Deep residual learning for image recognition," in *Proceedings of the IEEE conference on computer vision and pattern recognition*, 2016, pp. 770–778. IV-A, I
- [40] G. Huang, Z. Liu, L. Van Der Maaten, and K. Q. Weinberger, "Densely connected convolutional networks," in *Proceedings of the IEEE conference on computer vision and pattern recognition*, 2017, pp. 4700–4708. IV-A, I
- [41] X. Gu, H. Chang, B. Ma, S. Bai, S. Shan, and X. Chen, "Clothes-changing person re-identification with RGB modality only," *CoRR*, vol.

abs/2204.06890, 2022. [Online]. Available: <https://doi.org/10.48550/arXiv.2204.06890> II-B, IV-A, I